PTEP

Prog. Theor. Exp. Phys. **2019**, 013D02 (10 pages)
DOI: 10.1093/ptep/pty138

Coulomb breakup reactions of ^{93,94}Zr in inverse kinematics

Satoshi Takeuchi[1,2,*], Takashi Nakamura[1], Mizuki Shikata[1], Yasuhiro Togano[1], Yosuke Kondo[1], Junichi Tsubota[1], Tomoyuki Ozaki[1], Atsumi Saito[1], Hideaki Otsu[2], He Wang[2], Hiroyoshi Sakurai[2], Yukinobu Watanabe[3], Shoichiro Kawase[3,4], DeukSoon Ahn[2], Masayuki Aikawa[5], Takashi Ando[6], Shohei Araki[3], Sidong Chen[2], Nobuyuki Chiga[2], Pieter Doornenbal[2], Shuichiro Ebata[5], Naoki Fukuda[2], Tadaaki Isobe[2], Shunsuke Kawakami[7], Tadahiro Kin[3], Shunpei Koyama[6], Shigeru Kubono[2], Yukie Maeda[7], Ayano Makinaga[8,9], Masafumi Matsushita[4], Teiichiro Matsuzaki[2], Shin'ichiro Michimasa[4], Satoru Momiyama[6], Shunsuke Nagamine[6], Keita Nakano[3], Megumi Niikura[6], Kazuyuki Ogata[10,11], Takeshi Saito[6], Yoshiaki Shiga[2,12], Yohei Shimizu[2], Susumu Shimoura[4], Toshiyuki Sumikama[4], Pär-Anders Söderstrom[2], Hiroshi Suzuki[2], Hiroyuki Takeda[2], Ryo Taniuchi[6], Meiko Uesaka[2], Yasushi Watanabe[2], Kathrin Wimmer[4,6], Tatsuya Yamamoto[7] and Koichi Yoshida[2]

[1]*Department of Physics, Tokyo Institute of Technology, Tokyo 152-8551, Japan*
[2]*RIKEN Nishina Center, Saitama 351-0198, Japan*
[3]*Department of Advanced Energy Engineering Science, Kyushu University, Fukuoka 816-8580, Japan*
[4]*Center for Nuclear Study, University of Tokyo, RIKEN campus, Saitama 351-0198, Japan*
[5]*Faculty of Science, Hokkaido University, Hokkaido 060-0810, Japan*
[6]*Department of Physics, University of Tokyo, Tokyo 113-0033, Japan*
[7]*Faculty of Engineering, University of Miyazaki, Miyazaki 889-2192, Japan*
[8]*JEin Institute for Fundamental Science, NPO Einstein, Kyoto 606-8317, Japan*
[9]*Graduate School of Medicine, Hokkaido University, Hokkaido 060-8648, Japan*
[10]*Research Center for Nuclear Physics, Osaka University, Osaka 567-0047, Japan*
[11]*Department of Physics, Osaka City University, Osaka 558-8585, Japan*
[12]*Department of Physics, Rikkyo University, Tokyo 172-8501, Japan*
[*]E-mail: takesato@mail.nucl.ap.titech.ac.jp

Received October 19, 2018; Revised November 22, 2018; Accepted November 24, 2018; Published January 28, 2019

Coulomb breakup reactions of ^{93,94}Zr have been studied in inverse kinematics at incident beam energies of about 200 MeV/nucleon in order to evaluate neutron capture reaction methods. The ^{93}Zr(n,γ)^{94}Zr reaction is particularly important as a candidate nuclear transmutation reaction for the long-lived fission product ^{93}Zr in nuclear power plants. One- and two-neutron removal cross sections on Pb and C targets were measured to deduce the inclusive Coulomb breakup cross sections, 375 $\pm$ 29 (stat.) $\pm$ 30 (syst.) and 403 $\pm$ 26 (stat.) $\pm$ 31 (syst.) mb for ^{93}Zr and ^{94}Zr, respectively. The results are compared with estimates using the standard Lorentzian model and microscopic calculations. The results reveal a possible contribution of the pygmy dipole resonance or giant quadrupole resonance in the Coulomb breakup reactions of ^{94}Zr.

Subject Index D23, D50

1. Introduction

Nuclear data for long-lived fission products (LLFPs) have been investigated for several decades [1] since nuclear transmutation of LLFPs mixed in nuclear radioactive wastes is one of the candidate

techniques for the reduction of LLFPs and reuse of such elements with much lower radioactivity. Among the LLFPs, transmutations of ^{79}Se, ^{93}Zr, ^{107}Pd, and ^{135}Cs are important due to their long half-lives of 0.3M, 1.6M, 6.5M, and 2.3M years, respectively. These LLFPs can be transmuted to stable or short-lived nuclei by nuclear reactions, such as the neutron capture (n,γ) reaction, proton- and deuteron-induced spallation reactions, and fragmentation reactions. However, insufficient nuclear reaction data relevant to these isotopes are available due to experimental difficulties in handling LLFPs as targets and identifying the decay paths of LLFPs in these reactions. Such difficulties can be overcome by using LLFPs as a secondary beam in inverse kinematics. The possible reactions range from light-ion (proton, deuteron) induced to heavy-ion induced reactions such as the Coulomb breakup shown here. The secondary beam can be produced with the in-flight fission reaction of ^{238}U at intermediate to high beam energies. Since the reaction products are measured event-by-event, the cross sections for each reaction channel can be obtained individually.

Nuclear reaction experiments in inverse kinematics using LLFPs as secondary beams have been performed recently at the RIKEN Radioactive Isotope Beam Factory (RIBF) to accumulate nuclear reaction data for LLFPs [2–4]. In these experiments, proton- and deuteron-induced reactions were successfully applied for ^{90}Sr, ^{137}Cs, ^{93}Zr, and ^{107}Pd to measure isotopic-production cross sections. In the present paper we focus on the (γ,n) and (n,γ) reactions for ^{93,94}Zr. Neutron capture reactions on LLFPs are important approaches for nuclear transmutation. A measurement of the photo-absorption (γ,n) cross section ($\sigma_{\rm abs}$) can be associated with the (n,γ) cross section via the Hauser–Feshbach model combined with the Brink–Axel hypothesis [5,6]. Therefore a photo-absorption cross section measurement is an alternative method to obtain the (n,γ) cross section for LLFPs based on the statistical model calculation.

In this study, we use the Coulomb breakup reaction to extract the photo-absorption cross section. So far, photo-absorption cross sections have been extracted primarily by measuring the photo-neutron cross sections with real photons on stable nuclei [7–12]. Inelastic scattering with electrons and protons for stable nuclei have also been used [10–12]. The photo-absorption reaction relevant to the (n,γ) reaction appears at high excitation energies as a giant dipole resonance (GDR). The resonance shape around the neutron threshold energy is important to estimate the (n,γ) cross section. For unstable nuclei, Coulomb excitation/breakup is a useful tool, and has been applied to extract the (n,γ) cross sections and to study low-lying dipole strength [13–22]. The Coulomb breakup uses the excitation of a fast projectile by a virtual photon induced by a pulsed Coulomb field when it passes by a high-Z target. With this method, the photo-absorption cross section can be measured effectively for unstable nuclei while it is technically challenging to measure such a cross section with real photons on unstable nuclei. For unstable neutron-rich nuclei, we note that soft E1 excitation of halo nuclei [18,20–22] and pygmy dipole resonance (PDR) of neutron-rich nuclei [15,16,19] often make significant contributions to the photo-absorption cross section [23,24].

In the present study, we have measured the integral cross section of the Coulomb breakup reaction of the unstable ^{93}Zr and stable ^{94}Zr nuclei. For ^{94}Zr, there have so far been several experiments such as real-photon induced experiments [7,9]. We note that the giant resonance data for ^{94}Zr obtained by Berman et al. [7] are, in particular, useful in assessing the current technique. Systematic studies for photo-absorption cross sections via Coulomb breakup would be important not only for evaluating the nuclear data relevant to nuclear transmutation, but also for obtaining rich knowledge of nuclear structure, and nuclear reactions relevant to nucleosynthesis in the universe.

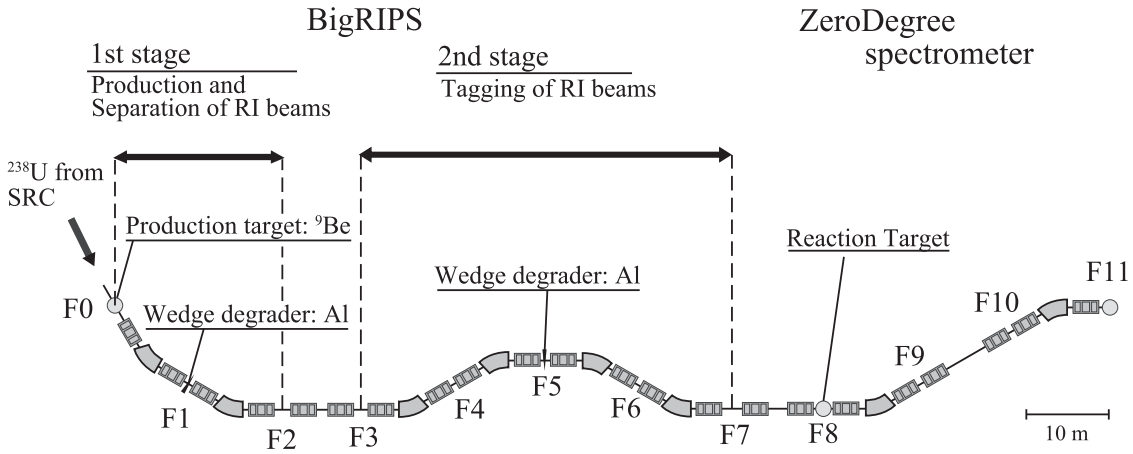

Fig. 1. Schematic illustration for BigRIPS and the ZeroDegree spectrometer.

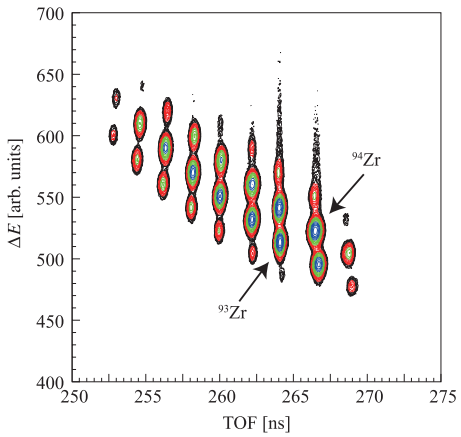

Fig. 2. Particle identification plot of secondary beams by TOF and ΔE in BigRIPS.

2. Experiment

The experiment was performed at the Radioactive Isotope Beam Factory (RIBF) operated by RIKEN Nishina Center and the Center for Nuclear Study, the University of Tokyo. A primary beam of ^{238}U at 345 MeV/nucleon with an intensity of 0.1 particle nA bombarded a ^{9}Be target with a thickness of 1 mm. Secondary beams of ^{93,94}Zr were produced by the in-flight fission reaction of ^{238}U and selected in the first stage of BigRIPS [25] with an Al wedge-type degrader of 2-mm thickness and a narrow momentum slit set to $\pm$ 1 mm ($\Delta p/p = \pm$ 0.047%) at the F1 focus (see Fig. 1). In the second stage of BigRIPS, the beam particles were further selected and identified event-by-event using the time-of-flight (TOF) and energy-loss (ΔE) method. An Al wedge-type degrader of 3.5-mm thickness was additionally installed at the F5 focus to further purify the ^{93,94}Zr nuclei in the secondary beams. The TOF of each beam particle was measured with plastic scintillators placed at the F3 and F7 foci with thicknesses of 0.2 mm each. ΔE was measured by the ionization chamber at F7, which was filled with P10 gas (mixed gas of 90% argon and 10% methane) at 650 Torr. Figure 2 shows a particle identification plot of the secondary beams. The beam purities of ^{93,94}Zr were about 7% and 10%, respectively, corresponding to intensities of about 110 and 150 Hz of the total beam intensity of 1.5k Hz. Secondary beam energies of ^{93,94}Zr at the entrance of the secondary target were 203 and 204 MeV/nucleon, respectively.

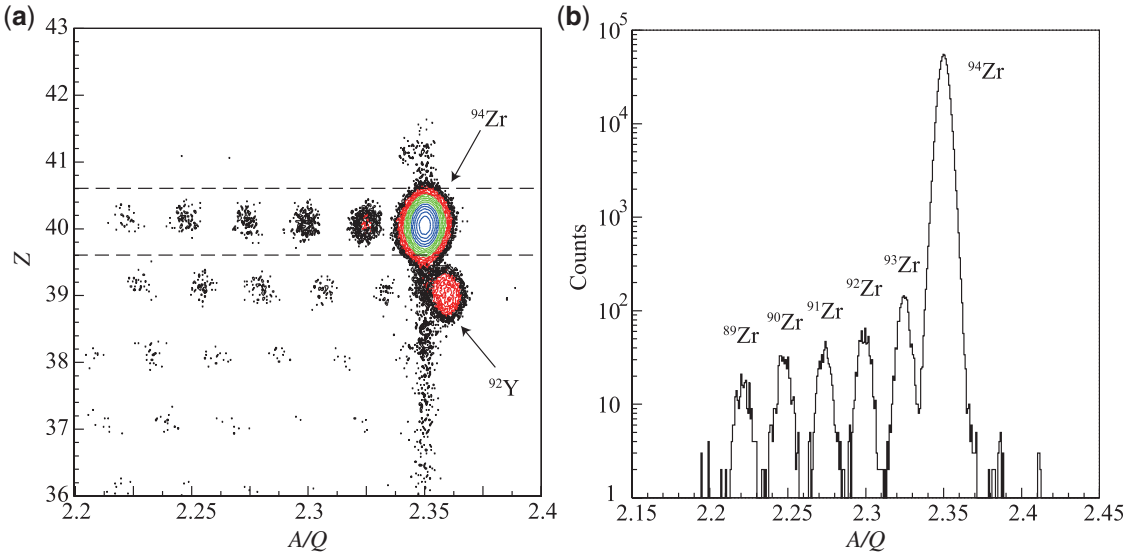

Fig. 3. (a) Particle identification plot of reaction products by mass-to-charge ratio (A/Q) and atomic number (Z) in the ZeroDegree spectrometer and (b) A/Q distribution for Zr isotopes. A gate on ^{94}Zr identified in BigRIPS has been applied to both plots. Dashed lines in (a) show the region of atomic number $Z = 40$ used in (b) as an atomic number gate.

^{93,94}Zr beams bombarded the secondary targets of Pb and C with thicknesses of 1.02 g/cm^2 and 0.61 g/cm^2, respectively, placed at the F8 focus. The reaction fragments were analyzed and identified by the ZeroDegree spectrometer (ZeroDegree) [25]. The particle identification in ZeroDegree was performed event-by-event by means of the TOF–ΔE–magnetic rigidity ($B\rho$) method. The TOF was measured by plastic scintillators at the F8 and F11 foci with 0.1- and 0.2-mm thicknesses, respectively. The ionization chamber, filled with P10 gas at 760 Torr, was installed at the F11 focus to measure the ΔE of the reaction fragments. Two parallel plate avalanche counters (PPACs) were installed at the dispersive focus F9 and the final achromatic focus F11. The positions and angles of reaction fragments measured at F9 were used to obtain the $B\rho$ value where the track of each ion was reconstructed using the information of the ion optics. Combining these observables, a particle identification plot for the reaction fragments in ZeroDegree was obtained as shown in Fig. 3(a).

Two $B\rho$ settings for ZeroDegree were applied to cover a wide range of momentum acceptance for the reaction fragments. In the first setting, the $B\rho$ value was adjusted to tune the non-reacted secondary beam to be centered (0% setting), which accepted momentum distributions down to -3% corresponding to the three-neutron removal channel from ^{94}Zr. In the other setting, the central $B\rho$ value was adjusted to be -3% in $B\rho$ relative to the 0% setting, which reaches down to the six-neutron removal channel of ^{94}Zr. These settings combined covered reaction fragments with $B\rho$ values from -6% to $+3\%$ relative to the non-reacted secondary beam. Yields of Zr isotopes observed at F9 (dispersive focus) were used to estimate the acceptance of the relevant Zr isotopes in ZeroDegree, which included momentum and angular contributions. The ZeroDegree acceptance was evaluated comparing the yield at the 0% setting with that at -3%. For the ^{93}Zr induced reaction, for instance, ^{93}Zr was centered for the 0% setting with 100% acceptance while ^{93}Zr was shifted to the higher-momentum side for the -3% setting. The ratio between yields of ^{93}Zr for these settings was used for the acceptance evaluation at the F9 position of 67.2 mm, corresponding to a momentum of $+3\%$.

Table 1. Breakup cross sections [mb] for Pb and C targets. Errors are statistical only.

	Pb target			C target		
	σ_{-1n} [mb]	σ_{-2n} [mb]	σ_{Sum} [mb]	σ_{-1n} [mb]	σ_{-2n} [mb]	σ_{Sum} [mb]
^{94}Zr	492 ± 21	156 ± 15	648 ± 25	84 ± 2	51 ± 2	135 ± 3
^{93}Zr	448 ± 24	159 ± 16	607 ± 29	80 ± 2	48 ± 2	128 ± 3

Table 2. Coulomb breakup cross sections [mb], σ_{-1n} and σ_{-2n}, for one- and two-neutron removal channels (-1n and -2n), respectively, and their sum. Errors show statistical (left) and systematic (right) uncertainties.

	σ_{-1n} [mb]	σ_{-2n} [mb]	σ_{Sum} [mb]
^{94}Zr	$341 \pm 21 \pm 19$	$62 \pm 15 \pm 12$	$403 \pm 26 \pm 31$
^{93}Zr	$303 \pm 24 \pm 18$	$72 \pm 16 \pm 11$	$375 \pm 29 \pm 30$

The lowest acceptance of 95% was obtained for ^{92}Zr in the ^{93}Zr+Pb run with a $B\rho$ setting of -3%, while the acceptances for the other isotopes were nearly 100%.

The charge-state distribution at the final focus F11 was estimated by the GLOBAL code [26]. This was then used to estimate the transmission efficiencies of the fully stripped states to F11, which were 90%, 93%, and 95% for the Pb, C, and empty target settings, respectively. These values take into consideration the effects of the reaction target and PPACs at the F8 and F9 foci. The charge-state ratio was also measured; this showed about 5% deviation from these calculations, and was included in the systematic errors in the Coulomb breakup cross sections shown below.

3. Results

The mass-to-charge ratio (A/Q) distribution of Zr fragments in the breakup of ^{94}Zr with the Pb target is shown in Fig. 3(b). Events with hydrogen- and helium-like charge states were removed using the position and angle information at F11, as those charge-state particles are not focused in the central position. The yield for each Zr isotope was deduced by fitting the A/Q distribution with Gaussian functions. Taking the acceptance and charge-state ratio into consideration, the breakup reaction cross sections for the one- and two-neutron removal (-1n and -2n) channels were extracted, as listed in Table 1. Background contributions from the beam-line detectors were estimated by measurements with the empty target holder, and were subtracted from the yields obtained with the Pb and C targets. The summed values of the -1n and -2n cross sections are also presented in Table 1.

Each Coulomb breakup cross section (σ_{CB}) was extracted by subtracting the nuclear breakup component estimated from the breakup cross section with the C target (σ_C) from that with the Pb target (σ_{Pb}) as

$$\sigma_{CB} = \sigma_{Pb} - \Gamma\sigma_C, \tag{1}$$

where Γ is a scaling factor. To evaluate Γ, a three-body model calculation for the breakup of ^{91}Zr by ^{12}C and ^{208}Pb targets at 200 MeV/nucleon has been carried out as in Ref. [27]. The nuclear potentials between the target and each constituent of ^{91}Zr, n or ^{90}Zr, were obtained by a microscopic folding model [28], in which nuclear density distributions by a Gogny D1S Hartree–Fock calculation [29] and the Melbourne G-matrix interactions [30] were adopted. The resulting value of Γ was 1.81 ± 0.23,

where the uncertainty was estimated by the accuracy of the four assumptions used in deriving Eq. (1); see Ref. [27] for details. Within the adopted three-body model, the value of Γ evaluated for ^{91}Zr is expected to be unchanged for ^{93}Zr and ^{94}Zr.

4. Discussion

The obtained Coulomb breakup cross sections are examined using the estimations based on 1) the GDR systematics, 2) the previous experimental data on ^{94}Zr, and 3) microscopic theoretical calculations. Here, first the photo-absorption cross sections were estimated for these three cases. Then, the Coulomb breakup cross sections were extracted using the equivalent photon method represented by

$$\sigma_{\mathrm{CB}} = \int \frac{N_{\mathrm{E1}}(E_x)}{E_x} \sigma_{\mathrm{abs}}(E_x) dE_x, \tag{2}$$

where N_{E1} and σ_{abs} respectively represent the virtual photon number and the absorption cross section for the E1 transition as a function of excitation energies (E_x) [31]. The first and second estimations use the standard Lorentzian model (SLO). In this model, $\sigma_{\mathrm{abs}}(E_x)$ can be approximated as

$$\sigma_{\mathrm{abs}}(E_x) = \frac{\sigma_\gamma E_x^2 \Gamma_\gamma^2}{(E_x^2 - E_\gamma^2)^2 + E_x^2 \Gamma_\gamma^2}, \tag{3}$$

where σ_γ, E_γ, and Γ_γ are the GDR parameters of the peak cross section, the resonance energy, and the resonance width, respectively.

In the first estimation (GDR systematics), E_γ and Γ_γ in Eq. (3) and its integral S_γ are parameterized as [32]

$$\begin{aligned} E_\gamma &= aA^{-1/3} + bA^{-1/6}\ [\mathrm{MeV}], \\ \Gamma_\gamma &= cE_\gamma^\delta\ [\mathrm{MeV}], \\ S_\gamma &= \frac{\pi}{2}\sigma_\gamma \Gamma_\gamma = 60 dNZ/A\ [\mathrm{mb \cdot MeV}], \end{aligned} \tag{4}$$

where, a, b, c, d, and δ are $a = 27.47(1)$, $b = 22.063(4)$, $c = 0.0277(4)$, $d = 1.222(2)$, and $\delta = 1.9$, respectively.

The second estimation is based on the data of the photo-neutron cross section of ^{94}Zr using real photons by Berman et al. [7] as shown in Fig. 4(a) (solid points). This can be a benchmark for the current study. The parameters E_γ, Γ_γ, and σ_γ in Eq. (3) to fit these data points were also presented in Ref. [7], and the fitted curve is shown by the blue solid curve in Fig. 4(a).

The third estimation is based on the microscopic calculations of the canonical-basis time-dependent Hartree–Fock–Bogoliubov (Cb-TDHFB) method [34] and the Hartree–Fock–Bogoliubov and QRPA (HFB+QRPA) method [32,35,36] for the GDR responses.

4.1. ^{94}*Zr*

The systematic GDR parameters of ^{94}Zr are calculated as $E_\gamma = 16.4(1)$ MeV, $\Gamma_\gamma = 5.62(12)$ MeV, and $\sigma_\gamma = 191(4)$ mb from Eqs. (4). The photo-absorption cross section using the systematic parameters is shown by the blue dotted line in Fig. 4(a), whose amplitude overestimates the experimental data by Berman et al. [7]. For these parameters, the Coulomb breakup cross section was extracted as 388(1) mb by integrating Eq. (2) over the excitation energy E_x from $S_{1\mathrm{n}} = 8.2$ MeV (one-neutron separation energy) to $S_{3\mathrm{n}} = 23.6$ MeV (three-neutron separation energy), to be compared with the

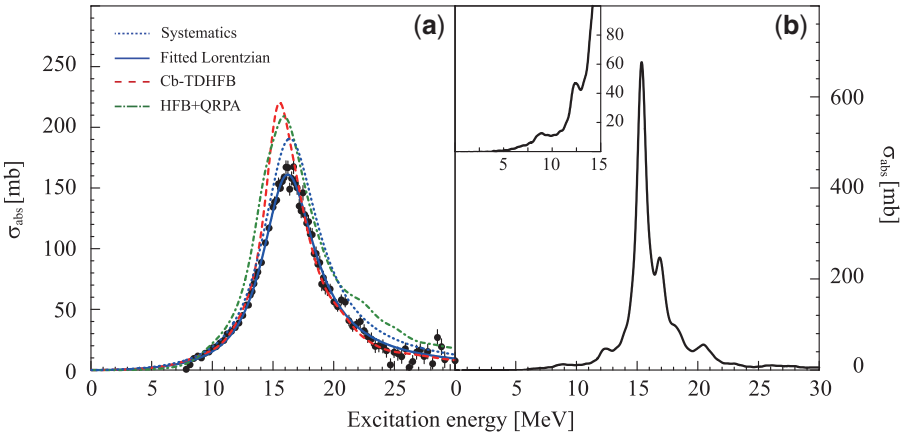

Fig. 4. (a) Photo-absorption cross section for ^{94}Zr. Dots and blue (solid) curve show the experimental results and the fitted Lorentzian with GDR parameters, respectively, obtained by Berman et al. [7]. Blue dotted, red dashed, and green dot-dashed curves show the Lorentzian curve with the systematic GDR parameters, and the results of microscopic calculations by Cb-TDHFB (the smoothing parameter $\Gamma = 3.0$ MeV) [34] and HFB+QRPA [32,35,36], respectively. (b) Photo-absorption cross section estimated by Cb-TDHFB using $\Gamma = 1.0$ MeV. The inset shows the low excitation energy region from 0 to 15 MeV.

sum cross section of σ_{-1n} and σ_{-2n}. This cross section exhausts 93% of the Thomas–Reiche–Kuhn (TRK) sum rule and is consistent with the current experimental result of 403 $\pm$ 26 $\pm$ 31 mb (see Table 3).

For the second evaluation using Berman's data, the Coulomb breakup cross section was extracted as 317(1) mb as listed in Table 3. Here, the GDR parameters in Eq. (2) were $E_\gamma = 16.20(4)$ MeV, $\Gamma_\gamma = 5.20(6)$ MeV, and $\sigma_\gamma = 161(4)$ mb from Berman's result, respectively, whose strength ($S_{1n} \leq E_x \leq S_{3n}$) is 74% of the TRK sum rule. The observed cross section is 86 $\pm$ 26 $\pm$ 31 mb larger than this estimation. Using the photo-neutron cross section spectra for the -1n and -2n channels in Ref. [7], we extracted the integral cross section for each channel as 276(3) mb and 58(1) mb, respectively. As shown in Table 2, the current σ_{-2n} value of 62 $\pm$ 15 $\pm$ 12 mb is consistent with Berman's value, while the current σ_{-1n} value of 341 $\pm$ 21 $\pm$ 19 mb is about 65 mb larger than Berman's σ_{-1n}. This shows that an enhancement compared to Berman's data occurs at lower excitation energy ($< S_{2n} = 14.9$ MeV).

In order to explain this enhancement of 65 mb, extra contributions from the other E1 contribution and/or the other multi-polarities such as M1 and E2 are investigated. When we assume that this discrepancy is fully due to the low-energy E1 strength such as PDR, the enhancement of 65 mb corresponds to the strength of 2.2 $\pm$ 0.7 $\pm$ 0.6% of the TRK sum rule with the assumption of $E = 8.8$ MeV and $\Gamma = 1.0$ MeV. Here, the assumed E and Γ are based on the Cb-TDHFB calculation with the Skyrme parameter set SLy4 [37] by Ebata et al. [33]. A peak cross section is 24 $\pm$ 8 $\pm$ 7 mb to reproduce this enhancement. In the case of $\Gamma = 3.0$ MeV, its strength is 3.0 $\pm$ 1.0 $\pm$ 0.8% of the TRK sum rule and a peak cross section is 13 $\pm$ 4 $\pm$ 4 mb. The existence of PDR in Zr isotopes has been reported for ^{90}Zr by Iwamoto et al. [39]. The energy and width were obtained by inelastic proton scattering as $E_{PDR} = 9.15(18)$ MeV and $\Gamma_{PDR} = 2.91(64)$ MeV, respectively, and its strength is 2.1(2)% of the TRK sum rule. This strength is close to the current estimations and may support the PDR contribution in ^{94}Zr. Recently, a photo-neutron cross section measurement of ^{94}Zr was performed by Utsunomiya et al. [9], who reported the existence of the M1 strength near the neutron separation energy. Since the Coulomb excitation/breakup reaction is not sensitive to the M1

Table 3. Comparison of the experimental Coulomb breakup cross sections [mb] of ^{93,94}Zr with those estimated by the calculations of the systematics; Berman's result; and two theoretical calculations, Cb-TDHFB and HFB+QRPA (see the main text). Integration was done for E_x from S_{1n} to S_{3n}.

Nucleus	present	systematics	Berman	Cb-TDHFB	HFB+QRPA
^{94}Zr	$403 \pm 26 \pm 31$	388 ± 1	317 ± 1	447	462
^{93}Zr	$375 \pm 29 \pm 30$	424 ± 1	–	453	475

strength, we exclude this contribution in this study. An alternative possibility for the enhancement of the observed cross section is the isoscaler giant quadrupole resonance (GQR), which can also be excited by the Coulomb breakup/excitation reaction [38]. Assuming that the enhancement is dominated by GQR, the strength is $51 \pm 16 \pm 15\%$ of the energy-weighted sum rule (EWSR) by the Lorentzian approximation for GQR with systematic parameters of $E_\gamma = 13.9$ MeV, $\Gamma_\gamma = 5.0$ MeV, and $\sigma_\gamma = 2$ mb [40]. The current result is compatible with the fraction of GQR in ^{94}Zr, which is 67(11)% obtained in the scattering measurement [41].

The theoretical calculations with Cb-TDHFB and HFB+QRPA are shown by the red dashed and green dot-dashed curves in Fig. 4(a). As shown in Table 3, the Coulomb breakup cross sections for $S_{1n} \leq E_x \leq S_{3n}$ were extracted as 447 mb and 462 mb, respectively, for these calculations. The Cb-TDHFB result is consistent with the current data, while the HFB+QRPA result is somewhat larger. The Cb-TDHFB result predicts a low-energy strength around 9 MeV for the photo-absorption cross section with the smoothing parameter $\Gamma = 1.0$ MeV, as shown in Fig. 4(b), while the photo-absorption cross section by the HFB+QRPA calculation was obtained from the Reference Input Parameter Library (RIPL-3) [32]; it does not include low-energy strength and is based on a spherical calculation. As the Cb-TDHFB result predicts a PDR fraction of about 1.3% of the total E1 strength, the consistency with the data may provide a hint of the existence of such a PDR.

4.2. ^{93}Zr

Since the GDR parameters for ^{93}Zr have not been experimentally determined so far because it is a radioactive isotope, data for ^{93}Zr were examined using the comparison with the GDR systematics and the microscopic calculations as applied to ^{94}Zr. The systematic GDR parameters of ^{93}Zr are calculated as $E_\gamma = 16.4(1)$ MeV, $\Gamma_\gamma = 5.65(12)$ MeV, and $\sigma_\gamma = 188(4)$ mb from Eqs. (4). The experimental value of $375 \pm 29 \pm 30$ mb is consistent with the extracted cross section of 424(1) mb using the systematic parameters with the strength ($S_{1n} = 6.7$ MeV $\leq E_x \leq S_{3n} = 22.6$ MeV) of 91% for the TRK sum rule.

For the theoretical evaluation using the microscopic calculations, Coulomb breakup cross sections were extracted based on the same procedures as ^{94}Zr. Cross sections were extracted as 453 mb and 475 mb using the Cb-TDHFB and HFB+QRPA calculations, respectively. Both results are slightly over the present result. No significant enhancement was observed in the present experiment for ^{93}Zr compared with the GDR systematics. If PDR and GQR exist, there are some contributions to the cross section as discussed for ^{94}Zr. For the discussion on the possible small PDR and GQR, cross section measurements by exclusive studies are desirable.

5. Summary and perspectives

We have measured Coulomb breakup reactions of the long-lived fission product ^{93}Zr and the stable ^{94}Zr isotope in inverse kinematics for the first time. Coulomb breakup cross sections were obtained

as 375 ± 29 (stat.) ± 30 (syst.) mb and 403 ± 26 (stat.) ± 31 (syst.) mb for ^{93}Zr and ^{94}Zr, respectively. The integral cross sections of Coulomb breakup reactions were investigated by comparing with the GDR systematics, the result of the previous experiment (for ^{94}Zr), and microscopic calculations (Cb-TDHFB, HFB+QRPA). The results show possible enhancements by pygmy dipole resonance and/or giant quadrupole resonance in ^{94}Zr. However, there are limitations in discussing the PDR and GQR contributions using integral cross sections based on inclusive measurements. For further discussions, a kinematically complete measurement of the breakup is required to deduce the energy-differential cross section by measuring all the decaying particles and γ rays by the invariant-mass method. Such a study would disentangle the contributions from GDR, PDR, and GQR to extract the photo-absorption cross section. Hence, we may evaluate the (n,γ) cross section using the obtained γ-ray strength function with an appropriate nuclear level density based on the Hauser–Feshbach model and the Brink–Axel hypothesis.

Acknowledgements

We would like to thank the RIBF accelerator staff for their stable operation during the experiment. This work was funded by the ImPACT Program of the Council for Science, Technology and Innovation (Cabinet Office, Government of Japan). This work was also supported in part by MEXT KAKENHI Grant No. 18H05404.

References

[1] IAEA, *Implications of Partitioning and Transmutation in Radioactive Waste Management*, Technical Reports Series No. 435 (2004).
[2] H. Wang et al., Phys. Lett. B **754**, 104 (2016).
[3] H. Wang et al., Prog. Theor. Exp. Phys. **2017**, 021D01 (2017).
[4] S. Kawase et al., Prog. Theor. Exp. Phys. **2017**, 093D03 (2017).
[5] D. M. Brink, Ph.D. Thesis, Oxford University (1955).
[6] P. Axel, Phys. Rev. **126**, 671 (1962).
[7] B. L. Berman, J. T. Caldwell, R. R. Harvey, M. A. Kelly, R. L. Bramblett, and S. C. Fultz, Phys. Rev. **162**, 1098 (1967).
[8] B. L. Berman and S. C. Fultz, Rev. Mod. Phys. **47**, 713 (1975).
[9] H. Utsunomiya et al., Phys. Rev. Lett. **100**, 162502 (2008).
[10] J. Speth and A. van der Woude, Rep. Prog. Phys. **44**, 719 (1981).
[11] A. van der Woude, Prog. Part. Nucl. Phys. **18**, 217 (1987).
[12] M. N. Harakeh and A. van der Woude, *Giant Resonances* (Oxford University Press, Oxford, UK, 2001), Oxford Studies in Nuclear Physics, Vol. 24.
[13] Á. Horváth et al., Astrophys. J. **570**, 926 (2002).
[14] U. Datta Pramanik et al., Phys. Lett. B **551**, 63 (2003).
[15] P. Adrich et al., Phys. Rev. Lett. **95**, 132501 (2005).
[16] O. Wieland et al., Phys. Rev. Lett. **102**, 092502 (2009).
[17] T. Nakamura et al., Phys. Rev. C **79**, 035805 (2009).
[18] T. Nakamura et al., Phys. Rev. Lett. **103**, 262501 (2009).
[19] D. M. Rossi et al., Phys. Rev. Lett. **111**, 242503 (2013).
[20] T. Nakamura et al., Phys. Rev. Lett. **112**, 142501 (2014).
[21] N. Kobayashi et al., Phys. Rev. Lett. **112**, 242501 (2014).
[22] N. Kobayashi et al., Phys. Rev. C **93**, 014613 (2016).
[23] T. Aumann and T. Nakamura, Phys. Scr. **T152**, 014012 (2013).
[24] T. Nakamura, H. Sakurai, and H. Watanabe, Prog. Part. Nucl. Phys. **97**, 53 (2017).
[25] T. Kubo et al., Prog. Theor. Exp. Phys. **2012**, 03C003 (2012).
[26] C. Scheidenberger, Th Stöhlker, W. E. Meyerhof, H. Geissel, P. H. Mokler, and B. Blank, Nucl. Instrum. Meth. B **142**, 441 (1998).
[27] K. Yoshida, T. Fukui, K. Minomo, and K. Ogata, Prog. Theor. Exp. Phys. **2014**, 053D03 (2014).
[28] K. Minomo, K. Washiyama, and K. Ogata, arXiv:1712.10121 [nucl-th] [Search INSPIRE].

[29] K. Minomo, K. Ogata, M. Kohno, Y. R. Shimizu, and M. Yahiro, J. Phys. G: Nucl. Part. Phys. **37**, 085011 (2010).
[30] K. Amos et al., Adv. Nucl. Phys. **25**, 275 (2000).
[31] C. A. Bertulani and G. Baur, Phys. Rep. **163**, 299 (1988).
[32] R. Capote et al., Nucl. Data Sheets **110**, 3107 (2009).
[33] S. Ebata, T. Nakatsukasa, and T. Inakura, Phys. Rev. C **90**, 024303 (2014).
[34] S. Ebata, T. Nakatsukasa, T. Inakura, K. Yoshida, Y. Hashimoto, and K. Yabana, Phys. Rev. C **82**, 034306 (2010).
[35] S. Goriely and E. Khan, Nucl. Phys. A **706**, 217 (2002).
[36] E. Khan et al., Nucl. Phys. A **694**, 103 (2001).
[37] E. Chabanat, P. Bonche, P. Haensel, J. Meyer, and R. Schaeffer, Nucl. Phys. A **627**, 710 (1997).
[38] J. Barrette et al., Phys. Lett. B **209**, 182 (1988).
[39] C. Iwamoto et al., Phys. Rev. Lett. **108**, 262501 (2012).
[40] W. V. Prestwitch, M. A. Islam, and T. J. Kennett, Z. Phys. A **315**, 103 (1984).
[41] Krishichayan, Y.-W. Lui, J. Button, D. H. Youngblood, G. Bonasera, and S. Shlomo, Phys. Rev. C **92**, 044323 (2015).